A Planar Compliance-Based Self-Adaptive MicrofluidVariable Resistor

Bozhi Yang and Qiao Lin, *Member, IEEE*

***Abstract*—This paper presents a self-adaptive microfluidic variable resistor that accomplishes passive control of liquid flows by exploiting the large compliance of elastomeric polymers such as polydimethylsiloxane. The device features a compliant microstructure embedded in a microchannel that consists of a flexible thin flap and a stiff stopper located in close proximity. The shape and size of the gap between the flap and stopper vary with the applied pressure, resulting in small resistance with respect to forward flow and large resistance with respect to reverse flow. The variable flow resistor shows an interesting diode behavior because its flow resistance is drastically different for different directions of applied pressures and is self-adaptive in the sense that its flow resistance varies with reverse pressure in such a way that the resulting flow rate remains a constant. That is, the flow resistor can be used as a check valve and, more importantly, a passive flow regulator. Prototype devices have demonstrated regulation of nearly constant water flow rates from 0.21 to 1.2 ml/min, with variations less than 3%, under driving pressures that vary significantly from 100 to over 200 kPa. Three-dimensional fluid-structure interaction simulations have been performed to investigate the interactions between the fluid flow and flap deflection. The simulation results agree with the experimental data and provide insight into the device characteristics. Based on its single-layer planar configuration, passive operation over a large pressure range, and use of a flexible and inexpensive polymer, this self-adaptive variable flow resistor is well suited to flow control in lab-on-a-chip systems. [2006-0129]**

***Index Terms*—Flow regulator, fluid structure interaction (FSI), fluidic resistor, microfluidics, valve.**

I. Introduction

MICRO flow control devices, such as those that guide, gate, drive, and regulate fluid flows, are important building blocks for miniaturized lab-on-a-chip systems [1], [2]. Such devices can be actively driven by on-chip or external actuators; alternatively, they can operate passively without actuation. Passive flow control devices do not require consumption of power or use of control circuitry, and hence, when compared with their active counterparts, are in general simpler, more reliable, and less expensive. For this reason, they are often preferred in practical lab-on-a-chip applications.

Manuscript received July 4, 2006; revised November 12, 2006. This work was supported in part by the National Science Foundation under Grant CTS-0304568. Subject Editor C. Liu.

B. Yang is with the Department of Mechanical Engineering, Carnegie-Mellon University, Pittsburgh, PA 15213 USA (e-mail: yangbozhi@yahoo.com).

Q. Lin was with the Department of Mechanical Engineering, Carnegie-Mellon University, Pittsburgh, PA 15213 USA. He is now with the Department of Mechanical Engineering, Columbia University, New York, NY 10027 USA (e-mail: ql2134@columbia.edu).

Color versions of one or more of the figures in this paper are available online at http://ieeexplore.ieee.org.

Digital Object Identifier 10.1109/JMEMS.2007.892892

Devices whose behavior distinctly depends on the characteristics of applied pressures comprise an important class of passive flow control components. Check valves, which allow unidirectional fluid flow, are a prominent example. The behavior of check valves is mainly determined by the direction of the applied pressure. Analogous to an electric diode in function, check valves are desired to have small flow resistance in one direction and orders-of-magnitude larger flow resistance in the other direction. Micro check valves have been fabricated using either solid-state materials [3]–[5] or various polymers such as parylene [6], SU-8 [7], and polydimethylsiloxane (PDMS) [8]. In general, polymers are attractive because of their low cost and flexible fabrication techniques. While some existing check valves use a planar geometry [9]–[12], most of them are nonplanar, which is not amenable to integration and generally requires complicated fabrication processes [3]–[5], [8].

Variable microfluidic resistors, whose flow resistance is a design-specified function of the applied pressure, are another type of pressure-dependent flow control devices. While the flow resistance of a fluid resistor can be actively adjusted by varying the cross-section [13] and length [14] of fluid channels, passive variable flow resistors, whose internal resistance changes with applied pressure by flow-induced changes of device geometry, have been scarce. Such devices, due to their passive, pressure-dependent flow resistance, can be used in fluidic logic circuits [15] or producing a desired relationship of the flow rate to the applied pressure. A particularly important instance of the latter case is flow regulation, i.e., maintaining flow rates at constant set points in the face of variable applied pressures. Flow regulators are of great utility for applications where constant flow rates are critical, such as controlled drug delivery systems [16], micro reactors [17], and microdialysis devices [18]. Passive flow regulation by variable resistors [19]–[23], whose resistance changes with pressure to produce a constant flow rate, is in general more attractive than active flow regulation [24]–[27]. It, however, has been rather challenging to design because the flow resistance must increase with the applied pressure in an approximately linear manner. One type of passive flow regulation device uses a flexural membrane covering a spiral-shaped channel etched in glass or silicon [19]–[21], wherein the channel cross-section diminishes under increasing pressure, thus leading to a largely steady flow rate. However, these devices are fragile and have relatively large dead volumes due to their complex geometry. A PDMS-based device has been recently reported for passive flow regulation, although it requires a three-dimensional configuration as well as a significant dead volume [22]. A planar PDMS device has also been reported, which is capable of maintaining largely constant flow rates of a polymer solution [23]. Since flow regulation is based on the polymer solution's vis-

coelasticity, the device functions only in applications that allow the use of polymer additives and non-Newtonian fluids. For the existing passive flow regulation devices [19]–[23], it is worth noting that there are significant variations in the regulated flow rate from the desired set point (over 15%), while the pressure range over which the regulators function is relatively small (less than 65 kPa of pressure variations).

This paper presents a passive microfluidic variable resistor that exploits compliant microstructures inside a microchannel in a planar configuration. The self-adaptive variable resistor shows a diode behavior because its flow resistance is drastically different for different directions of applied pressures. More importantly, it is self-adaptive in the sense that its flow resistance varies with reverse pressure to result in a nearly constant flow rate. Thus, it can be used not only as a check valve but also as a passive flow regulator. The variable resistor is structurally similar to a recently reported PDMS-based check valve [12] in the use of a compliant vertical flap. However, our device affords a much simpler single-layer fabrication process and is capable of the important function of passive flow regulation. To our knowledge, this is the first planar device for passive regulation of constant flow rates under varying applied pressures with no restriction on fluid constitutive properties. While our device can be optimized for either check valving or flow regulation by choice of material, structural shape, and dimensions, we have chosen to use a simple PDMS-based compliant structure, consisting of a flexible vertical flap near a stiff block, to demonstrate the variable flow resistor principle. Using PDMS as a structural material also offers the advantage of easy integration of the device within PDMS-based lab-on-a-chip systems. In addition to demonstrating the device's pressure-dependent flow resistance, we present the characterization of the device's compliant behavior under the action of the fluid flow, as well as initial results from the device simulation, which involves three-dimensional fully coupled fluid-structure interaction (FSI).

This paper is organized as follows. We will first describe the design and fabrication of the self-adjustable flow resistor (Section II). The modeling methodology, compliance characterization, microfluidic testing, and modeling results are then presented in Sections III–VI, respectively. A summary and a discussion of future work are given in Section VII.

II. Design and Fabrication

The microfluidic variable resistor has a single-layer planar configuration and consists of a passive, compliant structure embedded in a microchannel (Fig. 1). A thin compliant diaphragm, hereafter called a flap, is located perpendicular to the flow in close proximity to a stiff block. The block, of rectangular or other shapes, limits the deflection of the flap in one direction and is therefore called a stopper. The gap between the flap and stopper, which have the same height as the channel, restricts the passage of flow. Both the top and bottom of the flap are anchored to the respective channel walls, although this can be changed by choice of fabrication methods.

In response to a flow, the flap will be deflected either away from the stopper if the flow occurs in the forward direction or toward the stopper if the flow occurs in the reverse direction (Fig. 1). The flow resistance of the device depends on the size of the flap-stopper gap, which in turn depends on the flap deflection caused by the applied pressure. Under forward flow, the gap widens so that the flow resistance is small. On the other hand, under reverse flow, the flap approaches and eventually comes into contact with the stopper, leading to drastically increased flow resistance. It follows that the device possesses the characteristics of a diode and can be used as a check valve.

More importantly, the flow resistance is a function of the pressure drop over the device, and it is particularly interesting to observe this dependency when the device is subjected to a reverse flow. When the reverse pressure drop is sufficiently large, the flap comes into contact with the stopper. As the thin flap is anchored at three of its edges to the top, bottom, and one vertical wall of the channel, the flap-stopper gap effectively becomes two orifices, respectively, above and below the contact area, respectively (Fig. 1). As the pressure increases, the orifice size decreases, leading to an increased resistance to the flow. By proper choice of device design parameters, the tendency of this increased flow resistance to weaken the flow can cancel out the tendency of the increasing pressure to enhance the flow. As a result, the flow rate can remain a constant over a certain range of pressure drop. This self-adaptive variation of flow resistance thus allows the device to regulate a constant flow under variable pressures.

It is advantageous to fabricate the variable flow resistor from polymers for their excellent compliance properties. In particular, we chose to use PDMS, a highly compliant elastomeric polymer. Standard replica molding techniques [28], [29] were used to fabricate the PDMS prototype devices. The molding master, with inverted microchannel features, was first fabricated from a negative-tone SU-8 photoresist (SU-8 2100, MicroChem Corp., Newton, MA) on a silicon wafer using photolithography. Then a curing agent and PDMS prepolymer (Sylgard 184 Silicone Elastomer Kit, Dow Corning, weight ratio $A : B = 1 : 10$) was thoroughly mixed and degassed to remove entrapped air bubbles. A 1-min trimethylchlorosilane vapor treatment was applied to the molding master to facilitate later PDMS retrieval from the master mold. The mixture was next poured onto the mold and cured for 3 h at 100 °C in oven. The resulting PDMS sheet with resistor features was peeled off the master and bonded to a flat PDMS sheet or glass cover slip after plasma treatment of the bonding surfaces. This assembly was placed inside an isothermal oven at 60 °C for 30 min to enhance the bonding strength. The micrograph of a fabricated device is shown in Fig. 1(b).

III. Numerical Simulations

Numerical simulations are performed to understand the behavior of the microfluidic variable resistor. We describe the simulation methodology here; the simulation results will be presented in Sections IV and VI. When a pressure drop is applied to the device, the fluid flow will cause the flap to deflect. The deflection of the flap, as well as its contact with the stopper, will then further alter the flow field inside and near the flap-stopper gap. We perform numerical simulations of this highly nonlinear problem of FSI when the device is subjected to forward or reverse flow. Note that under reverse flow, the flap will come into contact with the stopper at sufficiently large pressures, and the

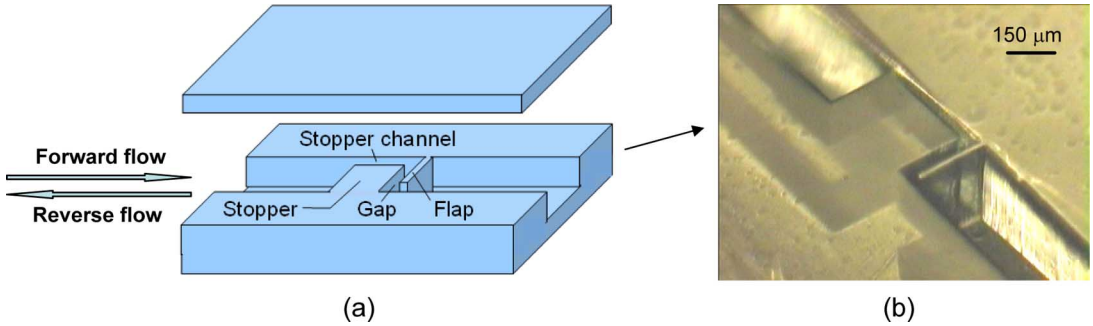

Fig. 1. Microfluidic variable resistor: (a) schematic design and (b) micrograph of a PDMS sheet with the resistor features.

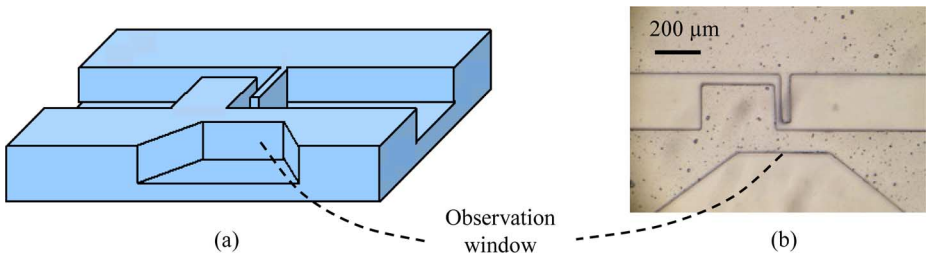

Fig. 2. (a) Three-dimensional schematic and (b) top-view optical micrograph of a device used for characterizing the flap compliance.

size and shape of the contact area is pressure-dependent. Simulation of fluid-structure interactions in the presence of flap-stopper contact is an extraordinarily difficult problem. Therefore, we will focus on the interaction of the flap deflection and the reverse fluid flow at pressures that are sufficiently small to not cause contact to occur. This significantly simplifies the simulation problem yet still allows us to observe those characteristics of reverse-flow device operation that are qualitatively different from forward flow mode.

The fully coupled interactions between fluid flow and flap deflection are simulated using the ANSYS® multifield solver [30]. The simulation involves a three-dimensional domain consisting of the fluid as well as the structure, with their interfaces constantly deforming because of the flap deflection. In addition, the nonlinear elasticity of the structural material (PDMS) and the large strain involved in the flap deflection are considered. During simulations of the device under either forward or reverse flow, the pressure drop between the device inlet and outlet is applied in small increments, as is necessary for solution of nonlinear continuum mechanics problems. At each pressure increment, three-dimensional simulations of computational fluid dynamics (CFD) and structural deformations are iteratively carried out to compute flow field and flap defection. These simulations are based on the following assumptions. The fluid, taken to be water, is incompressible and Newtonian with constant density (1000 kg/m^3) and viscosity (10^{-3} Pa $\cdot$ s). The flow is laminar as the Reynolds number is estimated to be less than 1000 for all devices over pressure ranges of interest. PDMS is modeled as an isotropic, incompressible hyperelastic material [31]. Such a material is nonlinearly elastic with its constitutive law given in terms of a strain energy density function $W = C_1 I_1 + C_2 I_2$, where I_1 and I_2 are the first and second invariants of the Finger deformation tensor [32]. For PDMS, we choose $C_1 = 70.9$ and $C_2 = 45.5$ kPa, which correspond to a nominal Young's modulus of $E = 6(C_1 + C_2) = 700$ kPa [32], defined as the derivative of uniaxial stress with respect to uniaxial strain at zero strain.

IV. Characterization of Compliance

This section discusses measurements and simulation of the flap deflection under both forward and reverse pressures to gain insight into the device compliance. Challenges in observing flap deflection arose mainly from the three-dimensional curved shape of the deflected flap. In particular, the maximum deflection occurred near the center, rather than the top, of the flap. Thus, any attempt to observe the maximum deflection with the chip plane perpendicular to the microscope optical axis would be severely impeded by optical focusing difficulties. The decrease in image contrast due to the motion of the fluid also hinders deflection observation. These challenges were overcome by viewing the flap deflection from one side of the channel, allowed by a specially designed prototype device, in which a side-view observation window was placed near the flap's free end (Fig. 2). The device's channel width and height were 300 and 275 μm, respectively. The channel wall associated with the side-view window was 125 μm thick and was considered sufficiently stiff when compared with the compliant flap, which was 266 μm wide and 55 μm thick and was located at a distance of 30 μm from the stopper. The stopper channel had a width of 40 μm and a length of 500 μm.

The flap deflection under various pressures can be observed in the device's side-view micrographs as shown in Fig. 3, in which dashed lines have been added to guide the eye in viewing the gap and contact surface between the flap and the stopper. In the absence of an applied pressure, the flap is undeformed, and there is a straight gap between the flap and the stopper Fig. 3(a). In the case of forward flow, the deflection of the flap is not limited by the stopper and consistently increases with the applied forward

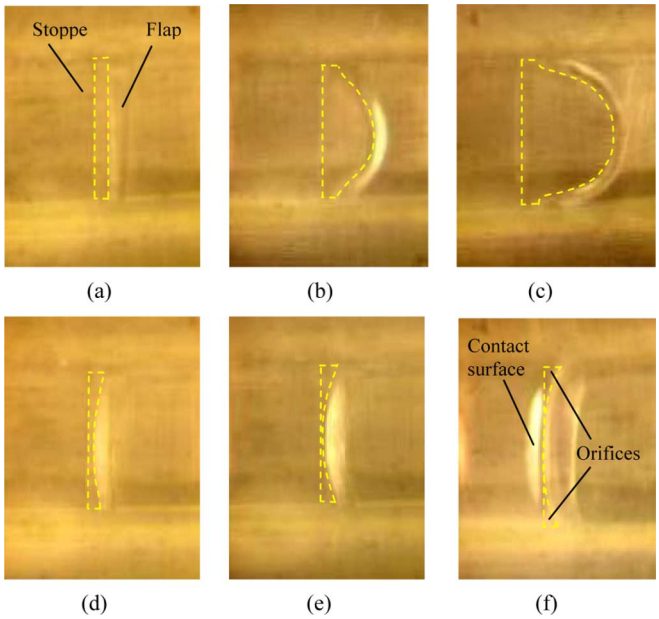

Fig. 3. Side-view micrographs showing flap deflection under various pressures. (a) Original flap shape. (b) and (c) Flap deflection under forward pressure. (d)–(f) Flap deflection under reverse pressure. (a) $\Delta p = 0$ kPa (0 psi), (b) $\Delta p = 68.9$ kPa (10 psi), (c) $\Delta p = 206.8$ kPa (30 psi), (d) $\Delta p = -13.8$ kPa (-2 psi), (e) $\Delta p = -34.5$ kPa (-5 psi), and (f) $\Delta p = -137.9$ kPa (-20 psi).

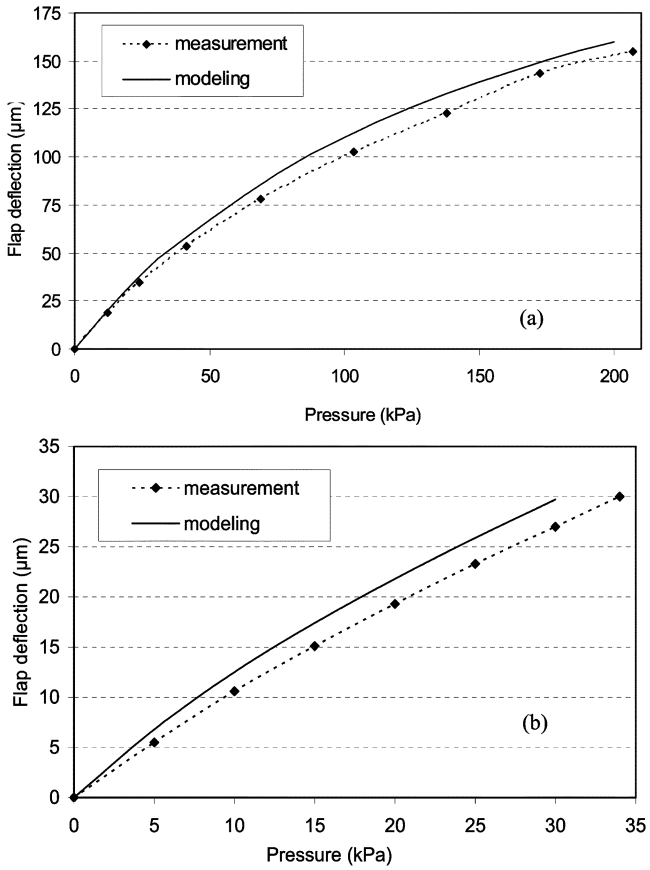

Fig. 4. Measured and simulated flap deflection under (a) forward and (b) reverse flow.

pressure [Fig. 3(b) and (c)]. Thus, the flap-stopper gap widens with increasing forward pressure. As a reverse pressure is applied, the flap is initially deflected toward the stopper [Fig. 3(d)]. As the reverse pressure increases to about 34.5 kPa (5 psi), the flap is deflected significantly such that it starts to contact the stopper [Fig. 3(e)]. In general, the critical pressure at which the flap contacts the stopper depends on the dimensions of the flap and the flap-stopper separation distance. As the reverse pressure further increases, the flap-stopper contact extends over a surface [Fig. 3(f)]. The bright area in Fig. 3(f) corresponds to the curved three-dimensional shape of the contact surface, which indicates that the stopper is actually also deformed due to the large compliance of PDMS. These observations confirm that the flap-stopper gap decreases with increasing reverse pressure. For sufficiently large pressures, the flap effectively forms two orifices above and below the contact area, respectively.

The measured maximum deflection at the tip of the flap, along with that obtained from the simulations, is plotted as a function of the applied pressure in Fig. 4. In the simulations presented here as well in Section VI, the inlet and outlet channels each had a length of 2 mm and equal cross-sectional dimensions to the device; the pressure drop over these channels is typically less than 1% of that over the flap-stopper section and hence negligible. It can be seen from Fig. 4 that the simulation and experimental results agree within 15% flow for forward flow and 20% for reverse flow. The deviations are perhaps caused by errors in the device dimensions and, more importantly, in the elastic properties of PDMS, used in the simulations. From the experimental and simulation results, we can clearly observe a nonlinear relationship between flap deflection and applied pressure, which is consistent with the fact that the flap deformations are in the large-deflection regime [33]. For example, at a forward pressure of 206 kPa (30 psi), the maximum deflection is 155 μm, nearly three times the flap thickness. This can also be seen from the relatively large values of the equivalent strain [32], which reaches about 0.2 under 30 kPa forward pressure near the flap's top and bottom edges where the flap is anchored to the channel ceiling and floor. We can also observe from Fig. 4(b) that the maximum deflection under reverse flow reaches 29.6 μm at a pressure of 30 kPa. As the initial flap-stopper distance is 30 μm, this implies that the flap tip is only 0.4 μm away from the stopper. That is, flap-stopper contact is imminent at this pressure.

V. Microfluidic Testing

Microfluidic testing was carried out using a setup in which pressurized argon was used to drive deionized water through the microfluidic device [Fig. 5(a)]. The device was held in a custom-designed package, which provided fluidic connection to the macro world Fig. 5(b). Pressure was measured upstream of the water tank and was either kept constant or allowed to vary with time using a voltage-controlled pressure regulator (SMC ITV 2000 series, Indianapolis, IN). Based on our calculations, the total pressure loss in the test setup and the microchannels leading to the compliant flap-stopper structure was on the order of hundreds of pascals, which was negligibly small compared to the driving pressure. Therefore, the pressure gauge readings gave the pressure drop across the flap-stopper structure. To measure flow rates smaller than 1 ml/min, a digital flowmeter (Alicat Scientific: L-1CCM-D, Tucson, AZ) was used. For flow

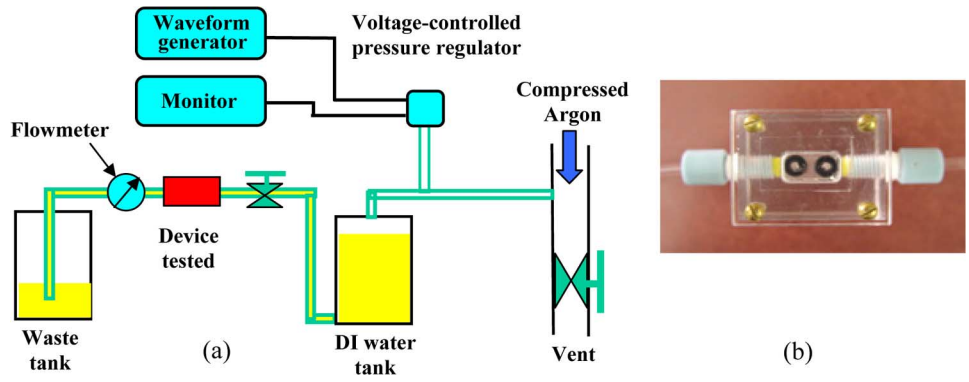

Fig. 5. (a) Schematic of the microfluidic test setup. (b) Custom-designed jig to hold the device to be tested.

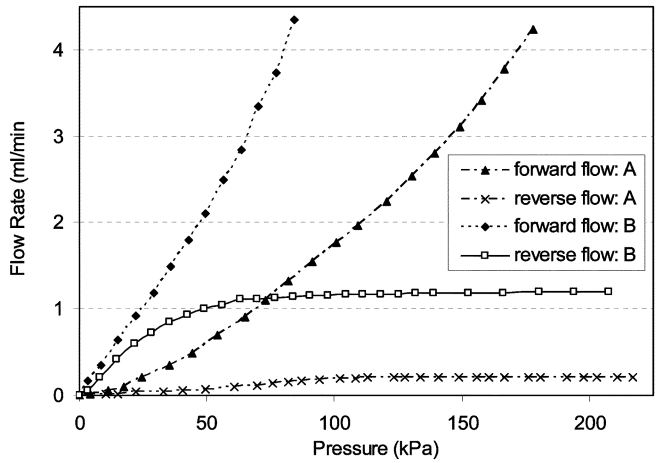

Fig. 6. Measured forward and reverse flow rate under static pressure for devices A and B.

rates larger than 1 ml/min, a laboratory flowmeter (Gilmont Instruments: GF-1160, Barrington, IL) was used. Flow rates were manually recorded.

Two prototype devices, referred to as devices A and B, were tested for their microfluidic characteristics. The devices were both based on a microchannel 300 μm wide and 275 μm high (as was the device used for compliance characterization above), and both had a flap 275 μm high and 266 μm wide, as well as a stopper channel 275 μm high, 40 μm wide, and 500 μm long. The flap in device A was 75 μm thick and located 25 μm from the stopper, while the flap in device B was 60 μm in thickness and located 36 μm from the stopper. The testing results obtained from these devices under forward and reverse flow are shown in Fig. 6. It can be seen that the forward flow rate increases consistently with the applied pressure and the reverse flow rate is very small under all pressures tested. This confirms that the device has the characteristics of a diode and can be used as a check valve. As expected, the size of the flap-stopper gap plays a key role in the device characteristics: a small gap will reduce the reverse flow rate although it also increases the forward flow resistance. Specifically, as the gap decreases from 36 μm (device B) to 25 μm (device A), the maximum leakage rate under reverse pressure is reduced by a factor of 6 from 1.2 to 0.21 ml/min, even though device A had a thicker flap than device B. Therefore, proper choice of the shape and dimensions of the flap-stopper structure can allow the device to function as check valves with desired performance specifications such as the leakage rate and diodicity [1], [2].

From the nonlinear functional relationship between the flow rate and pressure shown in Fig. 6, we can clearly observe the pressure-dependent flow resistance of the devices. In the case of forward flow, the flow resistance decreases with pressure, which can be attributed to the widening of the gap between the flap and the stopper as a result of the flap's being increasingly deflected away from the stopper. More importantly, the reverse flow resistance increases with pressure because of the narrowing and orifice formation in the flap-stopper gap. Thus, the reverse flow rate initially increases significantly with pressure and then becomes saturated. The pressure at which saturation occurs ranges approximately from 60 and 90 kPa for both devices. Upon saturation, the reverse flow rates remain nearly constant, respectively, at 0.21 ml/min (device A) and 1.2 ml/min (device B), with variations smaller than 3% at pressures up to more than 200 kPa. This compares favorably with existing micro flow regulators, for which the flow rate varies by 15% in a smaller pressure variation range (smaller than 65 kPa) [19]–[23].

Thus, the devices are self-adaptive in the sense that their flow resistance varies with the pressure to result in a constant flow rate over large pressure variations, achieving passive flow regulation.

The data presented in Fig. 6 were obtained from static measurements in the sense that the flow rate was measured at a series of fixed values of the reverse pressure. It will be interesting to investigate if the device is indeed capable of self-adaptive resistance variation and constant flow regulation when the pressure varies with time. For this purpose, we tested device A under time-dependent pressure variations. The capability of the microfluidic variable resistors functioning as a constant-flow regulator can be clearly seen in Fig. 7. The time-varying sinusoidal pressures had an average value of 155 kPa with fluctuation amplitude of 51.7 kPa and time periods of 4 and 2 min, respectively. The resulting flow rate under both pressure variations was nearly a constant, with an average value of 0.21 ml/min, consistent with results from fixed-pressure static measurements (Fig. 6). The standard deviation of the flow rate was 0.003 ml/min, or less than 2% of the average flow rate, for both time-varying pressure measurements.

These testing results have demonstrated the capability of the microfluidic variable resistor in regulating steady flow rates.

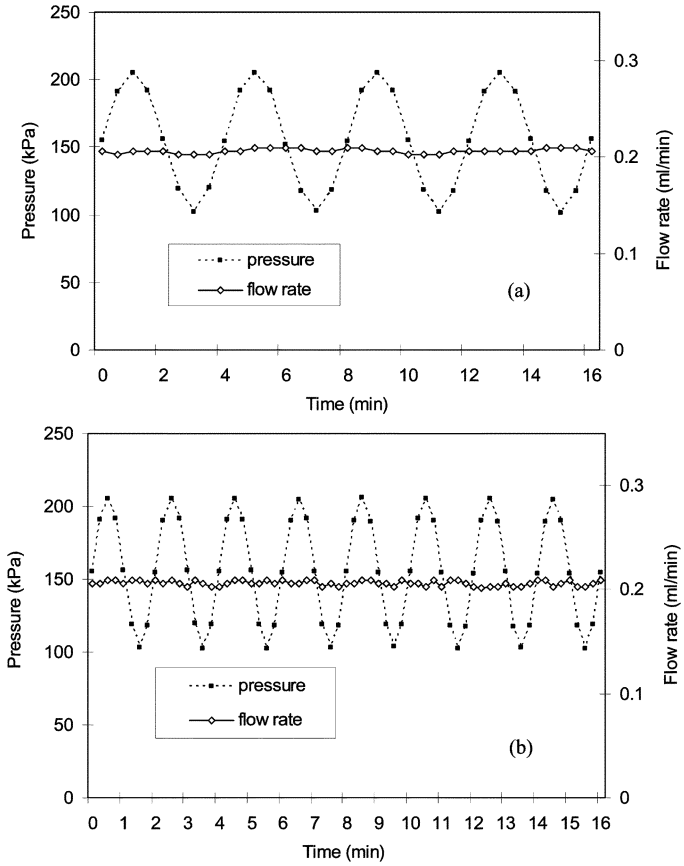

Fig. 7. Tested flow rate versus sinusoidal varying applied pressures for device A, where the period is (a) $\tau = 4$ min and (b) $\tau = 2$ min, respectively.

While the measurements were limited to relatively low pressure variation frequencies as flow rates were manually recorded, it is believed that the device is capable of flow regulation for pressure variations at considerably higher frequencies. This can be seen from an order-of-magnitude analysis. While this analysis holds for microfluidic variable resistors in general, specific numerical values will be calculated for concreteness based on the dimensions of device A. Here we note that if the flap vibration is quasi-static, then variations in the device's flow resistance will keep up with applied pressure variations to ensure flow regulation. In quasi-static flap vibrations, the effects of flap and fluid inertia, as well as hydrodynamic damping, are negligibly small compared with the effects of flap compliance. In this case, the flap deflection resulting from an applied time-varying pressure is predominantly determined by the flap compliance. The flap inertia is negligible if the pressure variation frequency f is small compared with the natural frequency of the flap f_n, which can be estimated by assuming the flap to be a flexural plate clamped at the three anchored edges [34]. The fluid flow in the flap-stopper gap can be approximated, for order-of-magnitude estimation purposes, as occurring between two rigid plates. One plate is fixed, representing the stopper. The other plate is attached to a spring with an elasticity constant $k = m(2\pi f_n)^2$ (where m is the flap mass), representing the compliant flap. The plates are nominally separated by h_0, which represents the flap-stopper gap associated with the dc component of the time-varying pressure. From lubrication theory [35], the fluid inertia is negligible if the pressure variation frequency f is small compared with $f_s = \nu/\left(2\pi h_0^2\right)$. In addition, the hydrodynamic damping effects are small compared with the flap compliance if $f = f_c = k/(2\pi c)$, where $c = \mu H w_f^3/h_0^3$ is the hydrodynamic damping coefficient [36]. Here, μ and ν are, respectively, the fluid's dynamic and kinematic viscosity and w_f and H are, respectively, the flap height and width. Taking h_0 to be one-third of the undeformed flap-stopper gap, and using typical material properties of water and PDMS [29], we can estimate, for device A, that $f_n \sim 35$ kHz, $f_s \sim 2$ kHz, and $f_c \sim 4$ kHz. It follows that if the pressure variation frequency is much lower than these characteristic frequencies—say, on the order of a few hundred hertz—the flap vibration will be quasi-static in nature and the device will be capable of flow regulation.

VI. Simulated Flow and Pressure Characteristics

The flow and pressure characteristics of the microfluidic variable resistor obtained from the three-dimensional FSI simulations will now be presented. We focus on device A, and the numerical simulation model includes inlet and outlet channels of the same dimensions as those for the device used in compliance characterization.

At a given pressure, FSI simulations yield the velocity field throughout the channel, which can be integrated to obtain the flow rate through the device. Thus, the flow rate can be computed as a function of the applied pressure. This calculated functional relationship, along with the experimental data, is shown in Fig. 8. Simulations are performed over the entire experimentally investigated pressure range (0–180 kPa) for forward flow Fig. 8(a) and for pressures ranging from 0 to 35 kPa, which is a pressure at which flap-stopper contact is imminent, for reverse flow Fig. 8(b). It can be seen that the simulations correctly predict the trend of both the forward- and reverse-flow experiments and agree with the experimental data within 15% for forward flow and 17% for reverse flow. The errors are likely caused by imprecise knowledge of device dimensions and PDMS's elastic properties (similar to Section IV), as well as deformations of the PDMS stopper and microchannel walls, which are not considered in the simulations.

To gain further insight into the device, we examine the calculated pressure distributions for both forward and reverse flow along a characteristic flow path defined by the serially connected segments A-B-C-D-E-F-G-H. Here, A, B, G, and H are located on the center line of the main channel, with A and H, respectively, 2 mm to the left and right of the flap-stopper structure and B 20 μm to the left and G 25 μm to the right of the structure. The segment C-D-E-F is the center line of the flow path formed by the flap and stopper and the main channel walls. The segments B-C and F-G are normal to the main channel's center line. The pressures along this path are normalized with the total pressure applied over the device (gauge pressure 50 kPa for forward flow and 35 kPa for reverse flow) and are shown in Fig. 9, where the abscissa corresponds to the path length measured from point A. It can be seen that in both forward and reverse flow cases, the pressure variations in the main channel (along the segments A-B and G-H) are very small, not exceeding 1% of the total pressure drop applied over the device. This is mainly because the

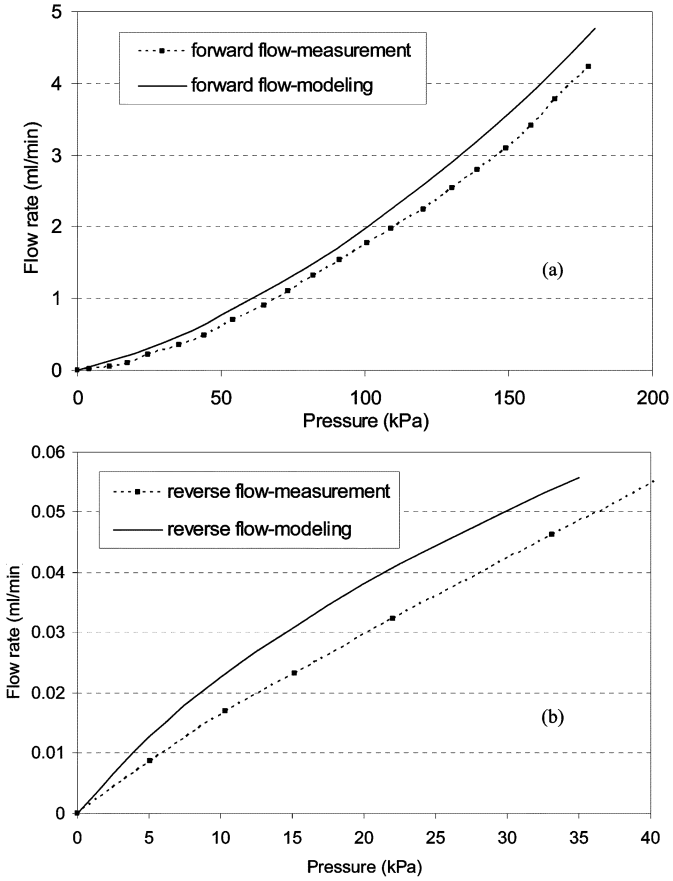

Fig. 8. Comparison of simulated and measured flow rates for device A: (a) forward flow and (b) reverse flow.

cross-section of the main channel is much larger than that of the stopper channel and flap-stopper gap.

Simulation results show that pressure drops in the flap-stopper gap and the stopper channel are significant. In the case of forward flow, as the hydrodynamic force causes the flap to deflect away from the stopper, the pressure drop in the flap gap is considerably smaller than that occurring in the stopper channel. That is, the pressure drop along D-E is 17% of the total pressure drop, compared with 71% for that along C-D. As indicated by the small negative normalized pressure values along F-G, the pressure outside the flap is slightly less than the outlet pressure as the fluid exits the flap-stopper structure. This arises from the recirculating flow associated with the sudden expansion of the flow passage at the exit of the flap-stopper gap [37]. It can also be seen from the simulation that since the pressure downstream from the flap-stopper structure, i.e., pressure along F-G-H, is very close to zero outlet pressure, the flap defection is largely determined by the pressure inside the flap-stopper gap, i.e., along D-E.

In the case of reverse flow along H-G-F-F-E-C-B-A, the relative significance of pressure drop in the flap-stopper gap and the stopper channel is reversed. That is, the pressure drop along E-D is 70% of the total pressure drop, compared with 29% for that along D-C. This indicates an increased flow resistance associated with the flap-stopper channel E-E for reverse flow compared to that for forward flow due to the narrowing of the flap

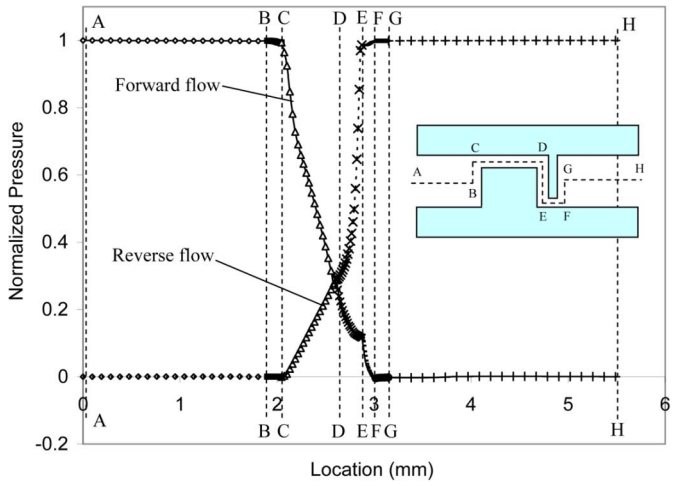

Fig. 9. Simulated normalized pressure distribution ($p_{\mathrm{local}}/p_{\mathrm{total}}$) along device A under forward ($p_{\mathrm{total}} = 50$ kPa) and reverse flow ($p_{\mathrm{total}} = 35$ kPa). (p_{total} is the total pressure applied across the inlet and outlet of the device).

gap under reverse flow. Similarly, the simulation shows that the pressure upstream from the flap-stopper gap is largely uniform and close to inlet pressure 50 kPa. Therefore, it is believed that the flap defection is essentially determined by the pressure inside the flap-stopper gap, i.e., along D-E.

Fig. 10 shows the simulated pressure distribution (over one half of the device) and velocity profile (shown in the axial plane of symmetry) for device A under 35 kPa of reverse pressure. It can be seen that for reverse flow, the pressure drop near the flap-stopper gap is much larger than the pressure drop along the stopper channel, mainly because of the narrowed effective flow pathway of the gap Fig. 10(a). The pressure drops along the inlet and outlet channels are very small because of the main channels' relatively large cross-section. The maximum velocity in the axial plane of symmetry occurs at the stopper channel's center line, and the flow profile is approximately parabolic across the stopper channel [Fig. 10(b)]. At the exit of the stopper channel, there is a recirculation zone due to the sudden expansion of the flow pathway.

VII. Conclusion

We have presented the design, fabrication, characterization, and modeling of a microfluidic variable resistor that accomplishes passive flow control by exploiting the large compliance of polymers such as PDMS. A compliant microstructure is embedded in a microchannel and consists of a flexible flap and a stiff stopper located in close proximity. The shape and size of the gap between the flap and stopper varies with applied pressure, resulting in small resistance with respect to forward flow and large resistance with respect to reverse flow. In addition, the reverse flow resistance variation is adaptive, in the sense that the flow rate is almost a constant under a certain range of variable reverse pressures. The variable resistor enables passive flow control functionalities such as valving and flow regulation. As a check valve, the self-adaptive resistor can efficiently realize a unidirectional fluid flow, in particular when the flap-stopper gap is small. Furthermore, exploiting passive adaptive variations of

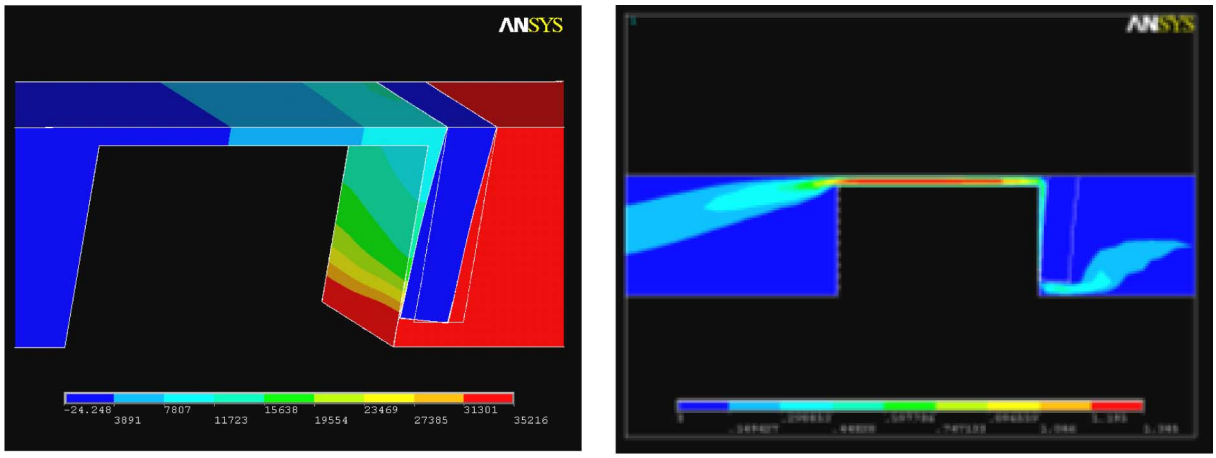

Fig. 10. Simulated (a) pressure over one-half the device and (b) velocity distributions in the axial plane of symmetry for device A under 35 kPa of reverse pressure.

the reverse flow resistance, the device can produce virtually constant flow rates in the face of significant variations in the driving pressure. The planar single-layer prototype can be fabricated by the standard replica molding technique from PDMS. Prototype devices have shown nearly constant water flow rates from 0.21 to 1.2 ml/min, with less than 3% variations, under driving pressures that vary significantly from 100 to more than 200 kPa. The device is well suited to flow control in lab-on-a-chip systems due to several significant features. The device is passive and simple in design, which leads to reduced power consumption requirements and improved robustness and reliability. The device's planar single-layer configuration and use of inexpensive polymers would greatly facilitate cost reduction and system integration. The small variation (less than 3%) in the regulated flow rate over a large pressure variation range (greater than 100 kPa) makes the device potentially useful even in applications with demanding flow regulation requirements. A fully coupled three-dimensional FSI modeling was conducted, which can accurately predict the trend of the flap deflection, flow rate, and pressure distribution of the devices.

There are several aspects that will be addressed in future work. First, while we have focused on simulations of fluid-structure interactions in the device when the flow is steady and when the flap is separated from the stopper, it will be interesting to extend these simulations to include the case where the flap and stopper are in contact with the flow. Flap–stopper contact is a highly nonlinear problem, and its coupling to CFD simulations is even more complex. This could be addressed by with numerical simulations that consider full coupling of fluid flow, structural deformations, and elastic contact. Alternatively, it might be possible to pursue a simplified approach that models the fluid flow in the flap–stopper gap using lubrication theory [35] and determines the flap–stopper gap shape and size using theory of elastic plates [33], [34]. Secondly, while we chose to use prototype devices with relatively large feature sizes to demonstrate the passive flow regulation principle, it will be interesting to investigate devices with scaled-down feature sizes. Such devices would have considerably increased flow resistance, and therefore under the same driving pressure variation ranges would produce drastically reduced flow rates compared with current prototype devices. Moreover, decreasing the flap-stopper gap size should significantly reduce the reverse flow rate, leading to improved diodicity for check-valve applications. It will also be interesting to experimentally measure the frequency response of such devices using an automated data acquisition system. Finally, the utility of the passive microfluidic variable resistors will be ultimately demonstrated by applications to practical microfluidic systems. For example, such a device could be used in check-valved micropumps and for flow regulation in such applications as drug delivery [16], microreactors [17], and microdialysis [18], where the availability of steady flow rates is crucial.

ACKNOWLEDGMENT

The authors would like to thank the MEMS Laboratory, Department of Electrical and Computer Engineering, Carnegie-Mellon University, for generously granting access to its fabrication and characterization facilities.

REFERENCES

[1] G. T. A. Kovacs, *Micromachined Transducers Sourcebook*. Boston, MA: WCB/McGraw-Hill, 1998.
[2] N. T. Nguyen and S. T. Wereley, *Fundamentals and Applications of Microfluidics*. Boston, MA: Artech House, 2002.
[3] A. Emmer, M. Jansson, J. Roeraade, U. Lindberg, and B. Hök, "Fabrication and characterization of a silicon microvalve," *J. Microcol. Separ.*, vol. 4, pp. 13–18, 1991.
[4] D. C. S. Bien, S. J. N. Mitchell, and H. S. Gamble, "Fabrication and characterization of a micromachined passive valve," *J. Micromech. Microeng.*, vol. 13, pp. 557–562, 2003.
[5] M. Hu, H. Du, S. F. Ling, Y. Fu, Q. Chen, L. Chow, and B. Li, "A silicon-on-insulator based micro check valve," *J. Micromech. Microeng.*, vol. 14, pp. 382–387, 2004.
[6] X. Q. Wang, Q. Lin, and Y. C. Tai, "A Parylene micro check valve," in *Proc. 12th IEEE Int. Workshop Micro Electro Mech. Syst. (MEMS '99)*, Orlando, FL, Jan. 17–21, 1999, pp. 177–182.
[7] N. T. Nguyen, T. Q. Truong, K. K. Wong, S. S. Ho, and C. L. N. Low, "Micro check valves for integration into polymeric microfluidic devices," *J. Micromech. Microeng.*, vol. 14, no. 14, pp. 69–75, 2004.
[8] N. L. Jeon, D. T. Chiu, C. J. Wargo, H. K. Wu, I. S. Choi, J. R. Anderson, and G. M. Whitesides, "Microfluidics section: Design and fabrication of integrated passive valves and pumps for flexible polymer 3-Dimensional microfluidic systems," *Biomed. Microdev.*, vol. 4, pp. 117–121, 2002.

[9] D. Kim and D. J. Beebe, "In-situ fabricated micro check-valve utilizing the spring force of a hydrogel," in *Proc. 7th Int. Conf. Micro Total Analysis Syst. (MicroTAS '03)*, Squaw Valley, CA, Oct. 5–9, 2003, pp. 947–950.
[10] E. F. Hasselbrink, Jr, T. J. Shepodd, and J. E. Rehm, "High-pressure microfluidic control in lab-on-a-chip devices using mobile polymer monoliths," *Anal. Chem.*, vol. 74, pp. 4913–4918, 2002.
[11] V. Seidemann, S. Butefisch, and S. Buttgenbach, "Fabrication and investigation of in-plane compliant SU8 structures for MEMS and their application to micro valves and micro grippers," *Sens. Actuators A: Phys.*, vol. 97, no. 8, pp. 457–461, 2002.
[12] M. L. Adams, M. L. Johnston, A. Scherer, and S. R. Quake, "Polydimethylsiloxane based microfluidic diode," *J. Micromech. Microeng.*, vol. 15, pp. 1517–1521, 2005.
[13] T. Goettsche, J. Kohnle, M. Willmann, H. Ernst, S. Messner, R. Steger, M. Storz, W. Lang, R. Zengerle, and H. Sandmaier, "Novel approaches to microfluidic components in high-end medical applications," in *12th Int. Conf. Solid State Sens., Actuators Microsyst. (Transducers '03)*, Boston, MA, Jun. 8–12, 2003, pp. 623–626.
[14] M. W. v. Toory and T. S. J. Lammerinky, "A novel micromechanical flow controller," *J. Micromech. Microeng.*, vol. 7, pp. 165–169, 1997.
[15] K. Foster and G. A. Parker, *Fluidics: Components and Circuits*. New York: Wiley-Interscience, 1970.
[16] B. Wang, T. J. Siahaan, and R. A. Soltero, *Drug Delivery: Principles and Applications*. Hoboken, NJ: Wiley, 2005.
[17] S. Dewitt, "Microreactors for chemical synthesis," *Current Opinion Chem. Biol.*, vol. 3, pp. 350–356, 1999.
[18] M. Müller, "Science, medicine, and the future: Microdialysis," *Clin. Rev.*, vol. 324, pp. 588–591, 2002.
[19] S. Park, W. H. Ko, and J. M. Prahl, "A constant flow-rate microvalve actuator based on silicon and micromachining technology," in *Tech. Dig. 1988 Solid-State Sens. Actuator Workshop (Hilton Head '88)*, Hilton Head Island, SC, Jun. 6–9, 1988, pp. 136–139.
[20] C. Amacker, Y. S. Leungki, V. Pasquier, C. Madore, M. Haller, and P. Renaud, "Passive micro-flow regulator for drug delivery system," in *Proc. Eurosensors XII*, Southampton, U.K., Sep. 13–16, 1998, pp. 591–594.
[21] P. Coussear, R. Hirschi, B. Frehner, S. Gamper, and D. Maillefer, "Improved micro-flow regulator for drug delivery systems," in *Proc. 14th IEEE Int. Conf. Micro Electro Mech. Syst. (MEMS '01)*, Interlaken, Switzerland, Jan. 21–25, 2001, pp. 527–530.
[22] E. P. Kartalov, C. Walker, C. R. Taylor, W. F. Anderson, and A. Scherer, "Microfluidic vias enable nested bioarrays and autoregulatory devices in Newtonian fluids," *Proc. Nat. Acad. Sci.*, vol. 103, pp. 12280–12284, 2006.
[23] A. Groisman, M. Enzelberger, and S. R. Quake, "Microfluidic memory and control devices," *Science*, vol. 300, pp. 995–998, 2003.
[24] A. Padmanabhan, C. Cabuz, E. Cabuz, J. Schwichtenberg, R. E. DeMers, and E. Satren, "MEMS-Based flow controller for flow cytometry," in *Tech. Dig. 2002 Solid-State Sens., Actuator Microsyst. Workshop (Hilton Head '02)*, Hilton Head Island, SC, Jun. 2–6, 2002, pp. 110–111.
[25] M. J. Mescher, C. E. Dub, M. Varghese, and J. O. Fiering, "Surface mount microfluidic flow regulator on a polymer substrate," in *Proc. 7th Int. Conf. Micro Total Anal. Syst. (MicroTAS '03)*, Squaw Valley, CA, Oct. 5–9, 2003, pp. 947–950.
[26] J. S. Fitch, A. K. Henning, E. B. Arkilic, and J. M. Harris, "Pressure-based mass-flow control using thermopneumatically-actuated microvalves," in *Tech. Dig. 1998 Solid-State Sens. Actuator Workshop (Hilton Head '98)*, Hilton Head Island, SC, Jun. 7–11, 1998, pp. 162–165.
[27] J. Xie, J. Shih, and Y. C. Tai, "Integrated surface-micromachined mass flow controller," in *Proc. 16th IEEE Int. Conf. Micro Electro Mech. Syst. (MEMS '03)*, Kyoto, Japan, Jan. 19–23, 2003, pp. 20–23.
[28] B. H. Jo, L. M. V. Lerberghe, J. N. Motsegood, and D. J. Beebe, "Three-dimensional micro-channel fabrication in poly-dimethylsiloxane (PDMS) elastomer," *J. Microelectromech. Syst.*, vol. 9, pp. 76–81, 2000.
[29] D. Armani, C. Liu, and N. Aluru, "Re-configurable fluid circuits by PDMS elastomer micromachining," in *Proc. 12th IEEE Int. Conf. Micro Electro Mech. Syst. (MEMS '99)*, Orland, FL, Jan. 17–21, 1999, pp. 222–227.
[30] E. Madenci and I. Guven, *The Finite Element Method and Applications in Engineering Using ANSYS*. New York: Springer-Verlag , 2005.
[31] E. M. Arruda and M. C. Boyce, "A three-dimensional constitutive model for the large stretch behavior of rubber elastic materials," *J. Mech. Phys. Solids*, vol. 41, pp. 389–412, 1993.
[32] C. W. Macosko, *Rheology: Principles, Measurement and Applications*. New York: VCH, 1994.
[33] S. Timoshenko *et al., Theory of Plates and Shells*, 2nd ed. New York: McGraw-Hill, 1959.
[34] A. W. Leissa, *Vibration of Plates*. Washington, D.C.: U.S. Government Printing Office, 1969.
[35] B. Hamrock, *Fundamentals of Fluid Film Lubrication*. New York: McGraw-Hill, 1994.
[36] Q. Lin, B. Yang, J. Xie, and Y. C. Tai, "Analysis of a surface-machined peristaltic pump," in *Proc. 8th Int. Conf. Micro Total Anal. Syst. (MicroTAS '04)*, Malmo, Sweden, Sep. 26–30, 2004, pp. 611–613.
[37] F. M. White, *Fluid Mechanics*, 5th ed. New York: McGraw-Hill, 2002.

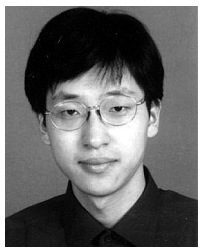

Bozhi Yang received the B.S. degree from Xi'an Jiaotong University, China, in 1997 and the M.S. degree from Tsinghua University, China, in 2000. He received the Ph.D. degree in mechanical engineering from Carnegie-Mellon University, Pittsburgh, PA, in 2006.

His thesis research was primarily on development and modeling of various micro flow control devices for biomedical applications. His doctoral research also included development of surface-tension-based microfluidic devices, humidity sensors, and integrated MEMS sensors for characterization and monitoring of biochemical processes. Since 2006, he has been a Senior Engineer in the Research and Engineering Center, Whirlpool Corporation.

Qiao Lin (S'97–A'98–M'02) received the Ph.D. degree in mechanical engineering from the California Institute of Technology (Caltech), Pasadena, in 1998.

His thesis research was on robotics. He conducted postdoctoral research in microelectromechanical systems (MEMS) at the Micromachining Laboratory, Caltech, from 1998 to 2000. He was an Assistant Professor of mechanical engineering at Carnegie-Mellon University, Pittsburgh, PA, from 2000 to 2005. He has been an Associate Professor of mechanical engineering at Columbia University, New York, since 2005. His research interests are in designing and creating integrated micro/nanosystems, in particular MEMS and microfluidic systems, for biomedical applications.